

Vision-based control for rigid body stabilization [★]

Rita Cunha ^a, Carlos Silvestre ^a, João Hespanha ^b, A. Pedro Aguiar ^a

^a*Department of Electrical Engineering and Computer Science, Institute for Systems and Robotics,
Instituto Superior Técnico, 1046-001 Lisbon, Portugal*

^b*Department of Electrical and Computer Engineering,
University of California, Santa Barbara, CA 93106-9560, USA*

Abstract

This paper addresses the problem of stabilizing to a desired equilibrium point an eye-in-hand system, which consists of a single camera mounted on a rigid body free to move on SE(3). It is assumed that there is a collection of landmarks fixed in the environment and that the image coordinates of those landmarks are provided to the system by an on-board CCD camera. The proposed method addresses not only the problem of stabilization but also that of maintaining feature visibility along the system's trajectory. The resulting solution consists of a feedback control law based on the current and desired image coordinates and reconstructed attitude and depth ratio information, which guarantees that *i*) the desired equilibrium point is an almost global attractor; *ii*) a set of necessary conditions for feature visibility holds throughout the system's trajectories; and *iii*) the image of a predefined feature point is kept inside the camera's field of view.

Key words: Vision-based control, nonlinear systems, asymptotic stabilization, perception and sensing

1 Introduction

Computer vision has long been recognized as an extremely flexible means of sensing the environment and acquiring valuable information for feedback control. Over the last few decades, awareness of this potential has brought about a widespread interest in the field of *vision-based control*, also known as *visual-servoing*. Vision-based control can be used to perform a variety of tasks such as positioning a manipulator's end-effector with respect to an object to be grasped (Cowan, Weingarten, and Koditschek, 2002; Deng, Janabi-Sharifi, and Wilson, 2005; Cheah, Liu, and Slotine, 2010) or landing an UAV over a predefined target (Ma, Soatto, Kosecka, and Sastry, 2004; Hamel and Mahony, 2007).

One of the main questions in vision-based control, which continues to challenge researchers, is the Field of View (FOV) problem. Although several recent papers address the problem explicitly, no definitive solution has been

proposed. As described in Cowan et al. (2002), the FOV problem presents two challenges: the features should not leave the image boundaries and they should also not become occluded by the object on which they are marked.

A wide range of different approaches has been put forward, which mostly only consider the problem of keeping the features inside the camera's FOV. Malis and Chaumette (2002) propose a solution whereby control of rotation is decoupled from that of position, using for that purpose the homography-based reconstruction of the orientation displacement between two views of a planar object, whose 3-D coordinates maybe unknown. To reduce the likelihood of feature loss, the control strategy keeps the centroid of the observed object inside the FOV. Cowan et al. (2002) develop a visual-servoing scheme based on a specific type of artificial potential function called navigation functions. Using the gradient vector field for a conveniently defined navigation function not only guarantees almost global convergence to the goal within the specified domain but also restricts the camera transient configurations to remain inside a predefined set, preventing the features from becoming occluded and leaving the FOV. For a 6-DOF body however, the navigation function is defined in the configuration space rather than in the image space. More recently, Lopes and Koditschek (2007) extend this approach to

[★] Corresponding author R. Cunha. Tel. +351-218418090. Fax +351-218418291.

Email addresses: rita@isr.ist.utl.pt (Rita Cunha),
cjs@isr.ist.utl.pt (Carlos Silvestre),
hspanha@ece.ucsd.edu (João Hespanha),
pedro@isr.ist.utl.pt (A. Pedro Aguiar).

control nonholonomic three degree of freedom kinematic systems. Chen, Dawson, Dixon, and Chitrakaran (2007) present an image-space path planner that tackles the FOV problem using once again navigation functions. The image-space navigation is defined such that the gradient points away from the feature loss scenario, but does not specifically avoid self-occlusions. Similarly to the classical image-based approach (Espiau, Chaumette, and Rives, 1992), determining the extent of the region of attraction for the resulting trajectory generator remains an open question. A number of recent methods combine classical image-based and position-based visual-servoing by either switching between the two (Gans and Hutchinson, 2007; Deng et al., 2005; Chesi, Hashimoto, Praticchizzo, and Vicino, 2004) or simultaneously driving both errors to zero (Gans, Hu, and Dixon, 2008). The switching rules are typically designed so as to keep the features in the FOV and simultaneously avoid large position and rotation errors. With these strategies, the stability of the system is difficult to analyze. For example, in (Gans and Hutchinson, 2007), asymptotic stability is guaranteed locally but no estimate of the region of attraction is provided. Chesi and Vicino (2004) also follow a path planning approach to address the FOV problem, using a circular-like trajectory generator to reduce translational displacements. García-Aracil, Malis, Aracil-Santonja, and Pérez-Vidal (2005) allow for some features to temporarily leave the FOV, using weight functions to guarantee the continuity of an image-based control law and obtain a result of local stability.

We propose a novel vision-based controller that guarantees almost global attractivity of the desired configuration defined in $SE(3)$. The approach adopted borrows from the work of authors like Koditschek (1989), Bullo and Murray (1999), Malisoff, Krichman, and Sontag (2006), Chaturvedi, McClamroch, and Bernstein (2009), and Cunha, Silvestre, and Hespanha (2008). Within this framework, rigid body configurations are expressed in their natural space, as elements of $SE(3)$, so as to avoid problems related to singularities or the so-called unwinding behavior (Bhata and Bernstein, 2000). The key novel contributions of this work with respect to the references above is that our results are not limited to guaranteeing rigid body stabilization. In fact, the key challenge addressed in this work is to find a stabilizing feedback controller that is guaranteed to keep the features visible and simultaneously provide a formal characterization of the region of the attraction for the resulting closed-loop system. For that purpose, our control algorithm relies on a two-stage controller based on the current and desired image coordinates and reconstructed orientation and depth ratio information that enforces necessary conditions for feature visibility throughout the closed-loop trajectories of the camera.

In contrast to most vision-based strategies, which only consider the problem of keeping the features inside the camera’s FOV (Malis and Chaumette, 2002; Gans and

Hutchinson, 2007; Chen et al., 2007), the proposed method also takes into account the second type of feature loss, which is due to self-occlusions. To this end, the necessary conditions for visibility are defined so that the camera not only points towards the features, but also remains in front of them. In addition, although there is no absolute guarantee that all feature points remain visible, the likelihood of maintaining feature visibility is reinforced by ensuring that a predefined feature point, such as the features’ centroid, is kept inside the FOV as it converges to the desired value. Finally, with the current approach we are not confronted with the difficult problem of local minima intrinsic to image-based strategies (Gans and Hutchinson, 2007; Chen et al., 2007; Deng et al., 2005), and therefore we can obtain a well defined region of attraction for the desired equilibrium point.

Similarly to (Malis and Chaumette, 2002; Chesi and Vicino, 2004; Chen et al., 2007), our solution does not require knowledge of the 3-D coordinates of the observed features and relies on the homography-based reconstruction method to recover the rotation and depth ratio between the current and desired views of a set of coplanar points. To enforce feature visibility, the two-stage controller first drives the position error to an arbitrarily small neighborhood of the origin, while pointing towards the feature points and only then ensures convergence in both position and orientation. Unlike other homography-based solutions that use the angle-axis representation for rotations, our second-stage controller for the rotation system uses directly the rotation matrix and more importantly defines an attractor for the rotation axis. This has a significant impact on the transients of the system, which is essential for enforcing feature visibility. The control law is complemented by an adaptive scheme to update the estimate of the desired depth and drive to zero the position error.

The paper is organized as follows. Section 2 introduces the vision-based control problem, derives necessary conditions to ensure feature visibility, and defines an image error vector. Section 3 describes the proposed vision-based controller. An exact expression for the region of attraction is derived in Section 3.1 and the transient configurations are shown to verify necessary conditions for feature visibility in Section 3.2. Simulation results that illustrate the behavior of the control system in the presence of image measurement noise and errors in camera calibration are presented in Section 4. A preliminary version of this paper was presented at the 46th IEEE Conference on Decision and Control (Cunha, Silvestre, Hespanha, and Aguiar, 2007).

2 Problem formulation

Consider a fully-actuated rigid-body, attached to a coordinate frame $\{B\}$ and let $(\mathbf{p}, R) = ({}^B\mathbf{p}_r, {}^B_r R) \in SE(3)$

denote the configuration of an inertial coordinate frame $\{I\}$ with respect to $\{B\}$, such that

$$\dot{\mathbf{p}} = -\mathbf{v} - S(\boldsymbol{\omega})\mathbf{p} \quad (1a)$$

$$\dot{R} = -S(\boldsymbol{\omega})R, \quad (1b)$$

where \mathbf{v} and $\boldsymbol{\omega} \in \mathbb{R}^3$ are the body-fixed linear and angular velocities, respectively and S denotes the map from \mathbb{R}^3 to the space of skew-symmetric matrices $\text{so}(3) = \{M \in \mathbb{R}^{3 \times 3} : M^T = -M\}$ defined so that $S(\mathbf{a})\mathbf{b} = \mathbf{a} \times \mathbf{b}$, where $\mathbf{a}, \mathbf{b} \in \mathbb{R}^3$ and \times denotes the cross product operator.

Consider also a desired configuration $(\mathbf{p}^*, R^*) \in \text{SE}(3)$, defined as the configuration of $\{I\}$ with respect to the desired body frame $\{D\}$, which is assumed to be fixed in the workspace, i.e. $\dot{\mathbf{p}}^* = 0$ and $\dot{R}^* = 0$. Introducing the error variables

$$\mathbf{p}_e = \mathbf{p} - \mathbf{p}^* \in \mathbb{R}^3, \quad R_e = RR^{*T} \in \text{SO}(3), \quad (2)$$

we can write the respective state equations as

$$\dot{\mathbf{p}}_e = -\mathbf{v} - S(\boldsymbol{\omega})(\mathbf{p}_e + \mathbf{p}^*) \quad (3a)$$

$$\dot{R}_e = -S(\boldsymbol{\omega})R_e, \quad (3b)$$

where \mathbf{v} and $\boldsymbol{\omega} \in \mathbb{R}^3$ are the body-fixed linear and angular velocities, respectively.

As illustrated in Figure 1, it is assumed that there is a collection of n feature points placed at fixed positions in the environment. The image coordinates \mathbf{y}_j and \mathbf{y}_j^* , $j \in \{1, 2, \dots, n\}$, acquired at the current and desired configurations (\mathbf{p}, R) and (\mathbf{p}^*, R^*) , respectively, are both available for feedback.

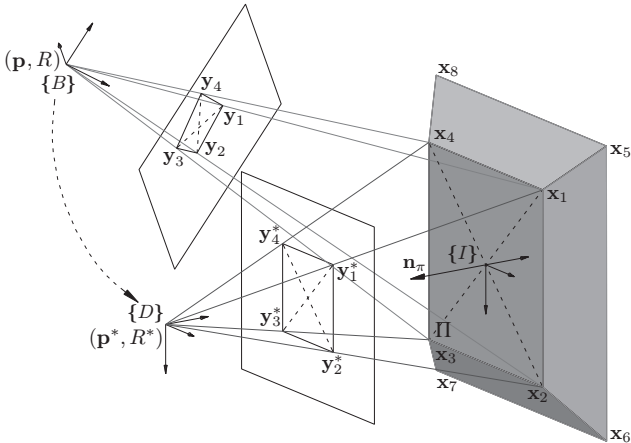


Fig. 1. Setup for the vision-based control problem.

The feature points, whose position coordinates in $\{I\}$, $\{B\}$, and $\{D\}$ are denoted by $\mathbf{x}_j \in \mathbb{R}^3$, $\mathbf{p}_j =$

$[x_j \ y_j \ z_j]^T \in \mathbb{R}^3$, and $\mathbf{p}_j^* = [x_j^* \ y_j^* \ z_j^*]^T \in \mathbb{R}^3$, $j \in \{1, 2, \dots, n\}$, respectively, are required to satisfy the following assumptions:

Assumption 1 *There are at least four coplanar points of which no three are collinear.*

Assumption 2 *All points are “below” a plane Π that contains the origin of $\{I\}$ and is orthogonal to \mathbf{n}_π .*

Using the perspective camera model, the image \mathbf{y}_j of the point \mathbf{p}_j can be written as

$$\mathbf{y}_j = \frac{1}{z_j} A \mathbf{p}_j \quad (4)$$

where $A \in \mathbb{R}^{3 \times 3}$ is the camera calibration matrix and z_j the unknown depth. Similarly, the image \mathbf{y}_j^* of \mathbf{p}_j^* is given by $\mathbf{y}_j^* = \frac{1}{z_j^*} A \mathbf{p}_j^*$. It is also convenient to define the images of the current and desired position vectors as

$$\mathbf{y} = \frac{1}{z} A \mathbf{p}, \quad \mathbf{y}^* = \frac{1}{z^*} A \mathbf{p}^* \quad (5)$$

respectively. Assuming that A is known, we assume without loss of generality that $A = I$ from now on.

For coplanar points, it is well known that the image pairs $(\mathbf{y}_j, \mathbf{y}_j^*)$ are related by a homography, which is the basis for a 3-D reconstruction algorithm (see for example (Faugeras and Lustman, 1988; Ma et al., 2004)). More specifically, we can write

$$\mathbf{y}_j = \frac{z_j}{z_j^*} H \mathbf{y}_j^*, \quad H = R_e + \frac{1}{d} \mathbf{t} \mathbf{n}^T \quad (6)$$

where $\mathbf{t} = \mathbf{p} - R_e \mathbf{p}^*$, $\mathbf{n} = -R^* \mathbf{n}_\pi$, and d is the desired distance to the feature plane that verifies $\mathbf{n}^T \mathbf{p}_j^* = d$. If Assumption 1 is verified, the homography matrix H is completely defined and the depth ratios z_j/z_j^* can be readily obtained (Malis and Chaumette, 2002). In particular, from \mathbf{y} and \mathbf{y}^* we can compute the depth ratio between the position vectors \mathbf{p} and \mathbf{p}^* defined as

$$\alpha = \frac{z}{z^*}. \quad (7)$$

In general, the decomposition of the homography matrix yields two valid solutions for the rotation matrix R_e and translation (up to a scale factor) between the two views. Additional images of the same scene or additional point correspondences in a different plane can be used to choose the correct solution (Faugeras and Lustman, 1988).

In view of the above, the primary control objective can be defined as that of designing a controller based on \mathbf{y} ,

\mathbf{y}^* , and reconstructed variables R_e and α that drives (\mathbf{p}, R) to (\mathbf{p}^*, R^*) . The proposed solution also relies on an adaptive scheme to update the desired depth estimate and estimate error denoted by

$$\hat{z}^*, \quad \tilde{z}^* = \hat{z}^* - z^* \in \mathbb{R},$$

respectively. For vision-based control systems, a simple convergence result is not sufficient to avoid failure, since the FOV problem needs to be explicitly addressed. Thus, we consider the additional goal of keeping the features inside the camera's FOV along the closed-loop system's trajectories.

As discussed in the introduction, feature loss can occur for two reasons: the features may either leave the camera's FOV or become occluded by the object on which they are marked (see for example the camera configuration $\{B_3\}$ shown in Figure 2). The likelihood of the first type of feature loss can be greatly reduced by ensuring that a relevant feature point remains in the FOV. For that purpose, we consider the image error given by the difference between the images of \mathbf{p} and \mathbf{p}^* , i.e.

$$\mathbf{y}_e = \mathbf{y} - \mathbf{y}^*. \quad (8)$$

Since \mathbf{p} is the position of the origin of the inertial frame $\{I\}$ expressed in the body frame $\{B\}$, it is important to place $\{I\}$ so that \mathbf{y}_e can provide an adequate measure for feature visibility. For example, the centroid of the feature points is a reasonable choice, provided that the image of the centroid, which in general does not coincide with the centroid of the image points, is available for feedback. In Section 4, we present a particular case where the image of the centroid can be readily obtained from the images of the feature points, even though none of the features points coincides with the centroid. Also note that even if \mathbf{y}_e is converging to zero, \mathbf{y} may become invalid if z goes to zero. Therefore, we introduce

$$z = \mathbf{e}_3^T \mathbf{p} > 0, \quad \mathbf{e}_3 = [0 \ 0 \ 1]^T, \quad (9)$$

as a necessary condition for keeping the features in the FOV.

To address the second type of feature loss, we introduce the requirement

$$\mathbf{n}_\pi^T \mathbf{p} = -\mathbf{n}_\pi^T R^T \mathbf{p} > 0, \quad (10)$$

to guarantee that the camera remains "above" the plane Π .

In summary, the problem addressed in this paper can be stated as follows:

Problem 3 Consider the rigid body kinematic model described in error coordinates by (1). Design a controller for \mathbf{v} and $\boldsymbol{\omega}$, based on \mathbf{y} , \mathbf{y}^* , R_e , and α , such that

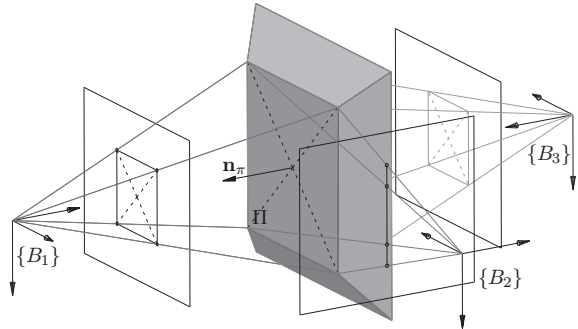


Fig. 2. Valid ($\{B_1\}$) and invalid ($\{B_2\}$ and $\{B_3\}$) configurations.

- i) $(\mathbf{p}_e, R_e) = (0, I_3)$ is an almost global attractor, meaning that its region of attraction \mathcal{R}_A coincides with $SE(3)$ except for a nowhere dense set of zero measure;
- ii) for every initial condition in a predefined set $\mathcal{J} \subset \mathcal{R}_A$, (9) and (10) are guaranteed to hold along the system's trajectories;
- iii) for sufficiently small errors on the initial depth estimate, the image \mathbf{y} is kept inside the FOV.

For the sake of completeness, we recall the definitions of almost global attractivity, and almost Global Asymptotic Stability (GAS) (Angeli, 2004; Chaturvedi, Bloch, and McClamroch, 2006) for a system of the form $\dot{x} = f(x)$. The equilibrium point $x = x^*$ is said to be an almost global attractor if the complement of its region of attraction is a nowhere dense set of measure zero. An almost GAS equilibrium point is an almost global attractor that is stable.

3 A Control Law for Visual-Servoing

In the following, we describe a solution to the problem of vision-based control. To this end, it is convenient to introduce the angle-axis representation for rotations, according to which $R_e = \text{rot}(\theta, \mathbf{n}) = I_3 + \sin \theta S(\mathbf{n}) + (1 - \cos \theta) S(\mathbf{n})^2$ represents a rotation of angle $\theta \in [0, \pi]$ about the unitary axis $\mathbf{n} \in \mathbb{S}^2$, and define the function $\text{sign} : \mathbb{R} \mapsto \{1, -1\}$ such that $\text{sign}(x) = 1$ if $x \geq 0$ and $\text{sign}(x) = -1$ if $x < 0$.

In loose terms, the proposed solution can be described as comprising two sequential steps:

- i) driving the position vector \mathbf{p} to an arbitrarily small neighborhood of \mathbf{p}^* ;
- ii) ensuring the convergence of (\mathbf{p}, R) to (\mathbf{p}^*, R^*) using a controller that also guarantees that $\mathbf{n}(t) \rightarrow \text{sign}(\mathbf{n}(0)^T \mathbf{n}_1) \mathbf{n}_1$ as $t \rightarrow \infty$, where $\mathbf{n}_1 = \mathbf{p}^* / \|\mathbf{p}^*\|$.

This strategy will allow for the definition of a set $\mathcal{J} \in SE(3)$ such that for all initial conditions in \mathcal{J} , both (9) and (10) are verified along the trajectories of the system.

The set \mathcal{J} depends on the desired configuration (\mathbf{p}^*, R^*) , the feature plane Π , and the initial estimate error for the desired depth $\tilde{z}^*(t_0) = \hat{z}^*(t_0) - z^*$. It is defined as

$$\mathcal{J} = \mathcal{J}_1 \cap \mathcal{J}_2 \setminus \mathcal{N}_A, \quad (11)$$

where \mathcal{N}_A is a zero measure set that will be explicitly defined shortly and

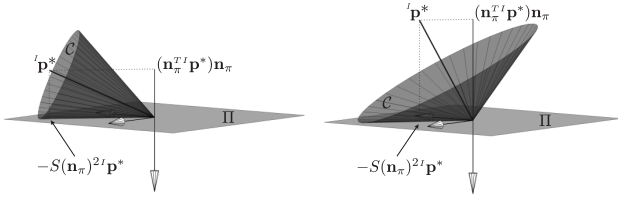
$$\mathcal{J}_1 = \{(\mathbf{p}_e, R_e) : z = \mathbf{e}_3^T(\mathbf{p}_e + \mathbf{p}^*) > 0\}, \quad (12)$$

$$\mathcal{J}_2 = \{(\mathbf{p}_e, R_e) : {}^I\mathbf{p} = -R^{*T}R_e^T(\mathbf{p}_e + \mathbf{p}^*) \in \mathcal{C} \text{ and } -R^{*T}R_e^T\mathbf{p}^* \in \mathcal{C}\}, \quad (13)$$

with the set $\mathcal{C} \subset \mathbb{R}^3$ given by

$$\mathcal{C} = \left\{ {}^I\mathbf{p} : {}^I\mathbf{p}^{*T}{}^I\mathbf{p} > \cos(\alpha_\pi - \epsilon) \|{}^I\mathbf{p}^*\| \|{}^I\mathbf{p}\|, \right. \\ \left. \alpha_\pi = \arccos\left(\frac{\|S(\mathbf{n}_\pi)^T \mathbf{p}^*\|}{\|{}^I\mathbf{p}^*\|}\right) \right. \\ \left. \epsilon = 2 \arctan\left(\frac{\sqrt{(z^*\gamma)^2 + \frac{\tilde{z}^*}{k_z} \tilde{z}(t_0)^2}}{\|{}^I\mathbf{p}^*\|}\right) \right\}. \quad (14)$$

As illustrated in Fig. 3, \mathcal{C} defines an unbounded cone in the space of inertial positions, which results from revolving the vector $-S(\mathbf{n}_\pi)^T \mathbf{p}^*$ (i.e. the projection of ${}^I\mathbf{p}^*$ onto to the feature plane) around ${}^I\mathbf{p}^*$. It is easy to see that \mathcal{C} is placed “above” the plane Π , and therefore (10) holds inside \mathcal{J}_2 . Also note that the opening angle of the cone has a maximum of $\alpha_\pi = \pi/2$ when ${}^I\mathbf{p}^*$ is perpendicular to the plane (in this case \mathcal{C} coincides with the half-space above the plane) and decreases to zero as ${}^I\mathbf{p}^*$ approaches the plane. Notice the difference between the cones depicted in Figures 3(a) and (b). The opening angle of \mathcal{C} is reduced by ϵ defined as a function of $\tilde{z}^*(t_0)$.



(a) ${}^I\mathbf{p}^* = [6 \ 6 \ 3.9]^T$; $\mathbf{n}_\pi = \mathbf{e}_3$ (b) ${}^I\mathbf{p}^* = [3 \ 3 \ 8]^T$; $\mathbf{n}_\pi = \mathbf{e}_3$

Fig. 3. Set $\mathcal{C} \subset \mathbb{R}^3$ for two different desired positions ${}^I\mathbf{p}^*$.

Having described the goals and properties of the proposed solution, a feedback law that yields this result can be constructed as follows:

1) Pick $M \in \mathbb{R}^{3 \times 3}$, such that $M = M^T \geq 0$, its two largest eigenvalues verify $\lambda_1 > \lambda_2 > 0$, and \mathbf{y}^* is an eigenvector of M associated with λ_1 .

2) Define the controller

$$\mathbf{v} = \begin{cases} k_1(\alpha\mathbf{y} - \mathbf{y}^*) & \text{until } \|\alpha\mathbf{y} - \mathbf{y}^*\| < \gamma \text{ (15a)} \\ k_2(\alpha\mathbf{y} - \mathbf{y}^*) - \hat{z}^* S(\boldsymbol{\omega})\alpha\mathbf{y} & \text{afterwards} \end{cases} \quad (15b)$$

$$\boldsymbol{\omega} = \begin{cases} k_3 S(\mathbf{y}^*)\alpha\mathbf{y} & \text{until } \|\alpha\mathbf{y} - \mathbf{y}^*\| < \gamma \text{ (16a)} \\ k_4 S^{-1}(R_e M - M R_e^T) & \text{afterwards} \end{cases} \quad (16b)$$

and the update law for \hat{z}^*

$$\dot{\hat{z}}^* = \begin{cases} 0 & \text{until } \|\alpha\mathbf{y} - \mathbf{y}^*\| < \gamma \text{ (17a)} \\ k_z \mathbf{y}^{*T} S(\boldsymbol{\omega})\alpha\mathbf{y} & \text{afterwards} \end{cases} \quad (17b)$$

where $S^{-1} : \text{so}(3) \mapsto \mathbb{R}^3$ denotes the inverse of the skew map S and $\gamma, k_1, k_2, k_3, k_4$, and k_z are positive scalars.

3.1 Stability Analysis

In this section, we analyze the stability of the closed-loop system and show that the first claim of Problem 3 is verified by the proposed controller, as stated in the following result.

Theorem 4 *Let Σ denote the closed-loop system that results from the feedback interconnection of (1) and (15)-(16), with \hat{z}^* as an exogenous input driven by (17). The point $(\mathbf{p}_e, R_e) = (0, I_3)$ is an almost global attractor of Σ and the corresponding region of attraction is given by $\mathcal{R}_A = \text{SE}(3) \setminus \mathcal{N}_A$, where*

$$\mathcal{N}_A = \left\{ (\mathbf{p}_{e0}, R_{e0}) : \mathbf{p}_e(t_0) = \mathbf{p}_{e0}, R_e(t_0) = R_{e0}, \right. \\ \left. \|\mathbf{p}_e(t_1)\| \leq z^*\gamma, \text{tr}(I_3 - R_e(t_1)) = 4, \right. \\ \left. \dot{\mathbf{p}}_e = k_1(\alpha\mathbf{y} - \mathbf{y}^*) - k_3 S(\mathbf{p})S(\alpha\mathbf{y})\mathbf{y}^*, \right. \\ \left. \dot{R}_e = k_3 S(S(\alpha\mathbf{y})\mathbf{y}^*)R_e, \text{ for } t_0 \leq t \leq t_1 \right\} \quad (18)$$

Moreover, $\mathbf{p}_e = 0$ is a global attractor of the position system and $R_e = I_3$ is an almost GAS equilibrium point of the rotation system. \square

To prove Theorem 4, we begin by focusing on the position system and then proceed to analyze the overall closed-loop system. Direct substitution of (15)-(16) in (1a) yields the following non-autonomous system for \mathbf{p}_e

$$z^* \dot{\mathbf{p}}_e = \begin{cases} -k_1 \mathbf{p}_e - k_3 \frac{1}{z^*} S(\mathbf{p}_e + \mathbf{p}^*)^2 \mathbf{p}^* & \text{until } \|\mathbf{p}_e\| < z^*\gamma, \\ -k_2 \mathbf{p}_e + \hat{z}^* S(\boldsymbol{\omega})(\mathbf{p}_e + \mathbf{p}^*) & \text{afterwards.} \end{cases} \quad (19a)$$

Lemma 5 *The position error system (19) with $\boldsymbol{\omega}$ and $\tilde{z}^* = \hat{z}^* - z^*$ as exogenous inputs given by (16b) and driven by (17b), respectively, has a global attractor at the origin.*

PROOF. Consider the Lyapunov function $V_1 = \frac{z^*}{2} \mathbf{p}_e^T \mathbf{p}_e$. Until the bound $\|\mathbf{p}_e\| < z^* \gamma$ is reached, \dot{V}_1 is given by

$$\dot{V}_1 = -k_1 \mathbf{p}_e^T \mathbf{p}_e + k_3 \frac{1}{z^*} \mathbf{p}_e^T S(\mathbf{p}^*)^2 \mathbf{p}_e \leq -k_1 \frac{2}{z^*} V_1$$

which implies that \mathbf{p}_e converges exponentially fast to the origin until the bound is reached. To analyze the stability of the second stage (19b), note that the time derivative of the Lyapunov function $V_2 = V_1 + \frac{(z^*)^2}{2k_z} (\tilde{z}^*)^2$ along the system trajectories is given by $\dot{V}_2 = -k_2 \mathbf{p}_e^T \mathbf{p}_e \leq 0$, which implies that \mathbf{p}_e and \tilde{z}^* are bounded and V_2 converges to a finite limit. Since in addition $\boldsymbol{\omega}$ given by (16b) is bounded, we have that $\dot{\mathbf{p}}_e$ given by (19b) is bounded and consequently \dot{V}_2 is bounded and \dot{V}_2 is uniformly continuous. Then, we can apply Barbalat's Lemma to show that \dot{V}_2 and consequently \mathbf{p}_e converge to zero. ■

Remark 6 *Until the bound $\|\mathbf{p}_e\| < z^* \gamma$ is reached, \mathbf{p}_e converges exponentially fast to the origin, which is exponentially stable. The closed-loop system will therefore always reach in finite time the bound $\|\mathbf{p}_e\| < z^* \gamma$. Once the bound is reached, the system begins a second stage ruled by the control laws (15b) and (16b) and update law (17b). Notice that no chattering will occur, given that there is no switching back to the first control laws (15a) and (16a), even if $\|\mathbf{p}_e\|$ becomes greater than $z^* \gamma$. During the second stage, \mathbf{p}_e continues to converge to zero and we can ensure that the bound $\|\mathbf{p}_e\|^2 < (z^* \gamma)^2 + \frac{z^*}{k_z} \tilde{z}^*(t_0)^2$ holds, given that the update law does not apply until this stage.*

To analyze the stability of the second stage, we present the following technical result.

Lemma 7 *Consider the feedback law for $\boldsymbol{\omega}$ given by*

$$\boldsymbol{\omega} = k_\omega S^{-1}(R_e M - M R_e^T), \quad (20)$$

where $M \in \mathbb{R}^{3 \times 3}$ is such that $M = M^T \geq 0$ and its two largest eigenvalues values verify $\lambda_1 > \lambda_2 > 0$. A possible choice for M is described in Section 4. Then, the interconnection of (3b) and (20) has an almost GAS equilibrium point at $R_e = I_3$ with region of attraction $\text{SO}(3) \setminus \{R_e : \text{tr}(I_3 - R_e) = 4\}$. Moreover, almost every initial condition $\mathbf{n}(0)$ for the axis of rotation $\mathbf{n}(t)$ converges asymptotically to $\text{sign}(\mathbf{n}(0)^T \mathbf{n}_1) \mathbf{n}_1$, where \mathbf{n}_1 is a unitary eigenvector of M associated with λ_1 . □

PROOF. For the sake of brevity, we present an outline of the proof, which uses results from Cunha et al. (2008). Consider the Lyapunov function $V = \text{tr}(I_3 - R_e)$, which can also be written as $V = 2(1 - \cos \theta)$ using the angle-axis representation for the rotation matrix R_e . Straightforward computations show that, along the trajectories

of the closed-loop system, \dot{V} is given by

$$\dot{V} = -\frac{1}{2} k_\omega V(4 - V) \mathbf{n}^T P \mathbf{n},$$

where P is the positive definite matrix given by $P = \text{tr}(M)I_3 - M$. Since V takes values between 0 and 4 and $\dot{V} < 0$ except for $V = 0$ and $V = 4$, we can conclude that $R_e = I_3$ is asymptotically stable and the set outside its region of attraction is given by $\{R_e : \text{tr}(I_3 - R_e) = 4\}$.

To show that almost every initial condition $\mathbf{n}(0)$ for the axis of rotation $\mathbf{n}(t)$ converges asymptotically to $\text{sign}(\mathbf{n}(0)^T \mathbf{n}_1) \mathbf{n}_1$, consider the closed-loop system for \mathbf{n}

$$\dot{\mathbf{n}} = k_\omega S(\mathbf{n})^2 P \mathbf{n} \quad (21)$$

and the Lyapunov function $W = 1 - \mathbf{n}_1^T \mathbf{n}$. In addition, let $\lambda_1 \geq \lambda_2 \geq \lambda_3 \geq 0$ denote the eigenvalues of M and \mathbf{n}_1 be such that $M \mathbf{n}_1 = \lambda_1 \mathbf{n}_1$. Simple algebra shows that $P \mathbf{n}_1 = (\lambda_2 + \lambda_3) \mathbf{n}_1$ and that if $\lambda_1 > \lambda_2 > 0$ then $\mathbf{n}^T P \mathbf{n} > \lambda_2 + \lambda_3$ for all $\mathbf{n} \in \mathbb{S}^2 \setminus \{-\mathbf{n}_1, \mathbf{n}_1\}$. Taking the time derivative of W , we obtain $\dot{W} = -k_\omega (\mathbf{n}^T P \mathbf{n} - (\lambda_2 + \lambda_3)(1 - W))$, which is negative definite for $W < 1$ or equivalently for $\mathbf{n}_1^T \mathbf{n} > 0$. It follows that $\mathbf{n} = \mathbf{n}_1$ is asymptotically stable and its region of attraction contains $\{\mathbf{n} : \mathbf{n}_1^T \mathbf{n} > 0\}$. The same argument but with $W = 1 + \mathbf{n}_1^T \mathbf{n}$ can be used to show that $\mathbf{n} = -\mathbf{n}_1$ is asymptotically stable and its region of attraction contains $\{\mathbf{n} : \mathbf{n}_1^T \mathbf{n} < 0\}$. Using (21), it is easy to show that $\mathbf{n}_1^T \dot{\mathbf{n}}(t) = 0$ defines an invariant set. As such, we can conclude that $\mathbf{n}(t)$ converges to $\text{sign}(\mathbf{n}(0)^T \mathbf{n}_1) \mathbf{n}_1$, provided that $\mathbf{n}(0)^T \mathbf{n}_1 \neq 0$. ■

PROOF. [Theorem 4] From Lemma 5, we have that $\mathbf{p}_e = 0$ is a global attractor of the position system (19). To analyze the rotation system, assume that the initial condition is given by $(\mathbf{p}_e(t_0), R_e(t_0))$ and the switching from the first to the second controller occurs at time $t_1 \geq t_0$. If $\|\mathbf{p}_e(t_0)\| \leq z^* \gamma$, the system is started directly inside the domain of application of the second controller (15b)-(16b), so that $t_1 = t_0$. It follows immediately from Lemma 7 and (16b) that $R_e = I_3$ is an asymptotically stable equilibrium point and that $R_e(t) \rightarrow I_3$ as $t \rightarrow \infty$, provided that $\text{tr}(I_3 - R_e(t_0)) \neq 4$. If $\|\mathbf{p}_e(t_0)\| > z^* \gamma$, $R_e(t_1)$ provides the initial condition for the second stage, which evolved from the initial condition $R_e(t_0)$ with an angular velocity $\boldsymbol{\omega}$ given by (16a). Using the same arguments of the first case, R_e converges to I_3 , provided that $\text{tr}(I_3 - R_e(t_1)) \neq 4$.

Putting together the results regarding the stability of \mathbf{p}_e and R_e , we can conclude that $(\mathbf{p}_e, R_e) = (0, I_3)$ is an almost global attractor of the closed-loop system and that the zero measure set \mathcal{N}_A outside its region of attraction is given by (18). ■

3.2 Necessary Conditions for Feature Visibility

In this section, we show that claims *ii*) and *iii*) of Problem 3 are also verified by the proposed controller. By analyzing the convergence behavior of the closed-loop system, we will be able to prove that the set \mathcal{J} defined in (11) verifies claims *ii*) of Problem 3. Next, we will show that for sufficiently small $\tilde{z}^*(t_0)$, the image \mathbf{y} remains inside the FOV.

Theorem 8 *Let Σ denote the system that results from the feedback interconnection of (3) and (15)-(16) and consider the set \mathcal{J} and angle α_π defined in (11) and (14), respectively. For all initial conditions $(\mathbf{p}_e(t_0), R_e(t_0)) \in \mathcal{J}$, the trajectories $(\mathbf{p}_e(t), R_e(t))$ of Σ with $t \geq t_0$ are such that $z(t) > 0$ and ${}^I\mathbf{p}^{*T}{}^I\mathbf{p}(t) > \cos \alpha_\pi \|{}^I\mathbf{p}^*\| \|{}^I\mathbf{p}(t)\|$.* \square

PROOF. Since \mathcal{J} results from the intersection of three sets $\mathcal{J} = \mathcal{R}_A \cap \mathcal{J}_1 \cap \mathcal{J}_2$, we consider each set separately. First we note that \mathcal{R}_A is positively invariant given that it is the region of attraction of the desired equilibrium point.

We can also show that \mathcal{J}_1 is positively invariant, meaning that the depth $z(t) = \mathbf{e}_3^T \mathbf{p}(t)$ remains positive if $z(t_0)$ is positive. While the first controller is being applied, the closed-loop system for \mathbf{p} can be written as

$$\dot{\mathbf{p}} = -\frac{k_1}{z^*}(\mathbf{p} - \mathbf{p}^*) - \frac{k_3}{z^{*2}}S(\mathbf{p})^2\mathbf{p}^*. \quad (22)$$

By noting that $\mathbf{p}^T S(\mathbf{p}^*)\dot{\mathbf{p}} = 0$, we can conclude that $\mathbf{p}(t)$ lives in the plane defined by \mathbf{p}^* and $\mathbf{p}(t_0)$. We can further restrict the region within which $\mathbf{p}(t)$ evolves from $\mathbf{p}(t_0)$ to \mathbf{p}^* , by selecting different values for k_1 and k_3 and analyzing the resulting solutions. With $k_1 = 0$, $\mathbf{p}(t)$ would have constant norm and move towards $\frac{\|\mathbf{p}(t_0)\|}{\|\mathbf{p}^*\|}\mathbf{p}^*$ through the shortest arc of circumference connecting $\mathbf{p}(t_0)$ to $\frac{\|\mathbf{p}(t_0)\|}{\|\mathbf{p}^*\|}\mathbf{p}^*$ (see Fig. 4). With $k_3 = 0$, $\mathbf{p}(t)$ would move along the straight line connecting $\mathbf{p}(t_0)$ to \mathbf{p}^* . As illustrated in Fig. 4, all other combinations for $k_1 > 0$ and $k_3 > 0$ result in solutions between these two limit trajectories, which indicates that $z(t) > 0$ if $z(t_0) > 0$. During the second stage, since $\|\mathbf{p} - \mathbf{p}^*\|^2$ does not grow beyond $(z^*\gamma)^2 + \frac{z^*}{k_z}\tilde{z}^*(t_0)^2$, sufficiently small γ and $\tilde{z}^*(t_0)$ guarantee that the depth $z(t)$ remains positive.

Considering now the set \mathcal{J}_2 , we recall that it can be identified with the set \mathcal{C} defined in (14) and analyze the time evolution of the inertial position vector ${}^I\mathbf{p} = -R^T\mathbf{p}$. Similarly to the previous case, we note that ${}^I\mathbf{p}$ and $R^T\mathbf{p}^*$ live in the same plane, since ${}^I\mathbf{p}^T S(R^T\mathbf{p}^*){}^I\dot{\mathbf{p}} = 0$ and ${}^I\mathbf{p}^T S(R^T\mathbf{p}^*)\dot{R}^T\mathbf{p}^* = 0$. Also we know that \mathbf{p} converges to \mathbf{p}^* , so ${}^I\mathbf{p}$ converges to a point on the sphere of radius $\|\mathbf{p}^*\|$. We can further restrict the region within which ${}^I\mathbf{p}$

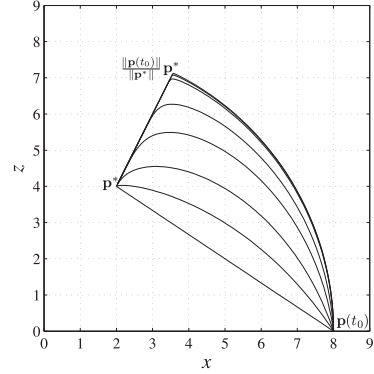


Fig. 4. Plane view of a set of solutions for (22) with desired position $\mathbf{p}^* = [2 \ 0 \ 4]^T$, initial condition $\mathbf{p}(t_0) = [8 \ 0 \ 0]^T$, $k_1 = 0.5$, and different gains $0 \leq k_3 \leq 10$.

evolves, by noting that when $\mathbf{p}(t_0)$ and \mathbf{p}^* are aligned, there is no rotational motion ($\boldsymbol{\omega} = 0$) and ${}^I\mathbf{p}$ moves along the straight line with the direction of $R(t_0)^T\mathbf{p}^*$. With $k_1 = 0$, there is no translational motion ($\mathbf{v} = 0$) and the body simply rotates to align \mathbf{p} with the direction of \mathbf{p}^* . With $k_3 = 0$, there is no rotational motion ($\boldsymbol{\omega} = 0$) and ${}^I\mathbf{p}$ moves along the straight line connecting ${}^I\mathbf{p}(t_0)$ and $R(t_0)^T\mathbf{p}^*$. Again, all other gain combinations result in solutions between these trajectories, implying that if ${}^I\mathbf{p}(t_0)$ and $R(t_0)^T\mathbf{p}^*$ start inside the cone \mathcal{C} defined in (14), ${}^I\mathbf{p}$ will remain inside that cone.

For the second stage, we consider a particular case and show that the intersection set $\mathcal{J}_2 \cap \{(\mathbf{p}_e, R_e) : \mathbf{p}_e = 0\}$ is positively invariant. Recalling that $\mathbf{p}_e = 0$ is an equilibrium point of the position error system, ${}^I\mathbf{p}$ can be written as ${}^I\mathbf{p}(t) = R^{*T}R_e(t)R^*{}^I\mathbf{p}^*$ for all $t > 0$ and the function $W : \text{SO}(3) \mapsto \mathbb{R}$ given by $W(R_e) = \mathbf{p}^{*T}(I_3 - R_e)\mathbf{p}^*$ takes the form $W({}^I\mathbf{p}) = {}^I\mathbf{p}^{*T}({}^I\mathbf{p}^* - {}^I\mathbf{p})$. The latter expression provides a useful interpretation for W , whose level curves can be plotted against the sphere of radius $\|{}^I\mathbf{p}^*\|$ as shown in Fig. 5. Intersecting the level curves of W with the cone \mathcal{C} , it is straightforward to observe that the nonincreasing monotonicity of W guarantees the positive invariance of $\mathcal{J}_2 \cap \{(\mathbf{p}_e, R_e) : \mathbf{p}_e = 0\}$. To

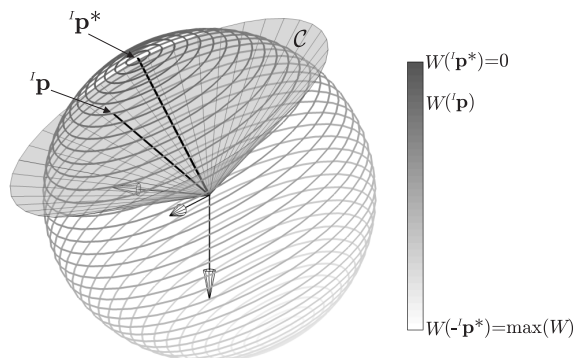


Fig. 5. Level curves for $W({}^I\mathbf{p})$, where ${}^I\mathbf{p} = R_e^T I \mathbf{p}^*$, intersected with \mathcal{C} .

show that $\dot{W} \leq 0$, recall that \mathbf{y}^* and consequently \mathbf{p}^* are eigenvectors of M associated with λ_1 . Then, \dot{W} can be written as $\dot{W} = -k_4 \mathbf{p}^{*T} (\lambda_1 I_3 - R_e M R_e) \mathbf{p}^* \leq 0$.

To extend this result to the case where $\mathbf{p}_e \neq 0$, consider by similarity with the cone \mathcal{C} , the definition of the set $\mathcal{C}[\mathbf{p}, \alpha]$ given by

$$\mathcal{C}[\mathbf{p}, \alpha] = \{\mathbf{u} : \mathbf{p}^T \mathbf{u} \geq \cos \alpha \|\mathbf{p}\| \|\mathbf{u}\|\}.$$

and let $t_1 \geq t_0$ denote the time when the switching to the second stage occurs. If ${}^I \mathbf{p}(t_1) \in \mathcal{C}[\mathbf{p}^*, \alpha_1]$ and $\mathbf{p}(t) \in \mathcal{C}[\mathbf{p}^*, \epsilon]$ for $t > t_1$, it follows that $-R(t_1)^T \mathbf{p}^* \in \mathcal{C}[\mathbf{p}^*, \alpha_1 + \epsilon]$. Using once again the Lyapunov function W , we can show that $-R(t)^T \mathbf{p}^* \in \mathcal{C}[\mathbf{p}^*, \alpha_1 + \epsilon]$ and consequently ${}^I \mathbf{p}(t) \in \mathcal{C}[\mathbf{p}^*, \alpha_1 + 2\epsilon]$ for $t > t_1$. Then, if $\alpha_1 + 2\epsilon < \alpha_\pi$, ${}^I \mathbf{p}(t)$ will stay inside the cone $\mathcal{C} = \mathcal{C}[\mathbf{p}^*, \alpha_\pi]$. ■

To conclude this section, we analyze the closed-loop system for the image error $\mathbf{y}_e = \mathbf{y} - \mathbf{y}^*$. Recall, that while the first controller (15a) and (16a) is being applied, the closed-loop system for \mathbf{p} is given by (22). Simple algebra shows that $\dot{\mathbf{y}}_e$ can be written as

$$\dot{\mathbf{y}}_e = -k_y \mathbf{y}_e, \quad k_y = \frac{k_1}{z} + k_3 \alpha \mathbf{y}^T \mathbf{y}. \quad (23)$$

Given that $z > 0$, we have that $\|\mathbf{y}_e\|$ is monotonically decreasing to zero and \mathbf{y} remains inside the FOV. After that, we rely on the bound on the position error $\|\mathbf{p}_e\|^2 < (z^* \gamma)^2 + z^* \tilde{z}^*(t_0)$ to guarantee that for a sufficiently small $\tilde{z}^*(t_0)$, \mathbf{y} does not leave the FOV as it converges to \mathbf{y}^* .

4 Simulation Results

The simulation results presented in this section illustrate the stability and convergence properties of the proposed vision-based controller in the presence of image measurement noise and camera calibration errors. To implement the feedback law (15)-(16) given the target configuration (\mathbf{p}^*, R^*) , we need to select both the matrix $M \in \mathbb{R}^{3 \times 3}$ and the set of feature points in the form of a matrix $X \in \mathbb{R}^{3 \times n}$, with $n \geq 4$.

The matrix M is required to be such that the two largest eigenvalues verify $\lambda_1 > \lambda_2 > 0$ and $M \mathbf{y}^* = \lambda_1 \mathbf{y}^*$. Defining the unitary vector $\mathbf{n}_1 = \mathbf{y}^* / \|\mathbf{y}^*\|$ and assuming that \mathbf{n}_1 and $\mathbf{e}_1 = [1 \ 0 \ 0]^T$ are not collinear, a possible choice for M is given by

$$M = USU^T, \quad (24)$$

$$U = \begin{bmatrix} \mathbf{n}_1 & \frac{S(\mathbf{n}_1)\mathbf{e}_1}{\|S(\mathbf{n}_1)\mathbf{e}_1\|} & \frac{S(\mathbf{n}_1)^2\mathbf{e}_1}{\|S(\mathbf{n}_1)^2\mathbf{e}_1\|} \end{bmatrix}, \quad S = \begin{bmatrix} \lambda_1 & 0 & 0 \\ 0 & \lambda_2 & 0 \\ 0 & 0 & \lambda_3 \end{bmatrix}.$$

Regarding X , it may seem that it can be formed by virtually any set of feature points satisfying Assumptions 1 and 2. However, since the visual-servoing problem is concerned with keeping feature visibility and the proposed solution only guarantees that (\mathbf{p}_e, R_e) stays inside \mathcal{J} , the matrix X should be carefully chosen. To meet the assumptions and ensure that the set \mathcal{J} does not lose its significance, we consider a set of $n = 8$ feature points such that

$$X = \begin{bmatrix} X_1 & X_2 \end{bmatrix}$$

$$X_1 = \begin{bmatrix} a_1 & a_1 & -a_1 & -a_1 \\ b_1 & -b_1 & -b_1 & b_1 \\ 0 & 0 & 0 & 0 \end{bmatrix}, \quad X_2 = \begin{bmatrix} a_2 & a_2 & -a_2 & -a_2 \\ b_2 & -b_2 & -b_2 & b_2 \\ -c & -c & -c & -c \end{bmatrix}$$

and $0 < a_1 < a_2$, $0 < b_1 < b_2$, and $c > 0$. Note that the choice of feature configurations is not limited to the one just proposed.

As shown in Fig. 6, the feature points correspond to the vertices of a polyhedron that results from chopping the top off a pyramid and the origin of $\{I\}$ coincides with the centroid of the polyhedron's upper face. By aligning

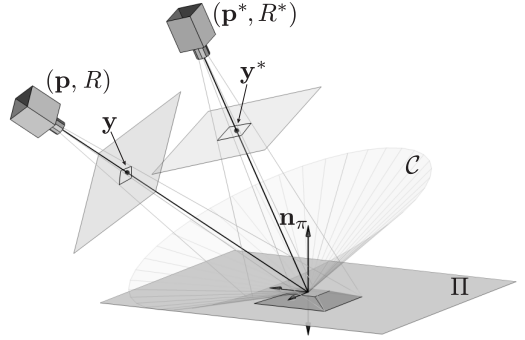
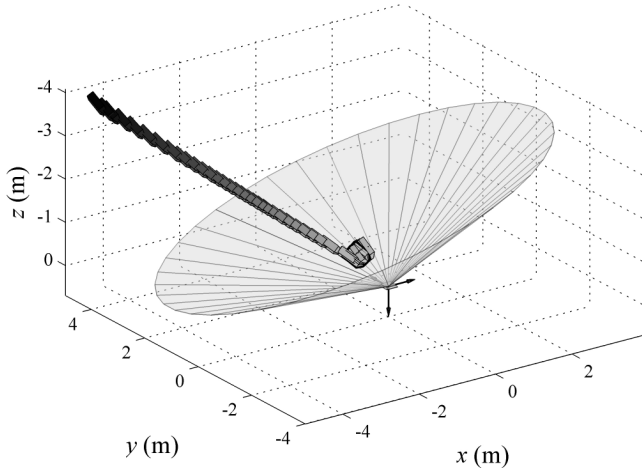


Fig. 6. Current configuration (\mathbf{p}, R) , desired configuration (\mathbf{p}^*, R^*) , and corresponding image coordinates \mathbf{y} and \mathbf{y}^* .

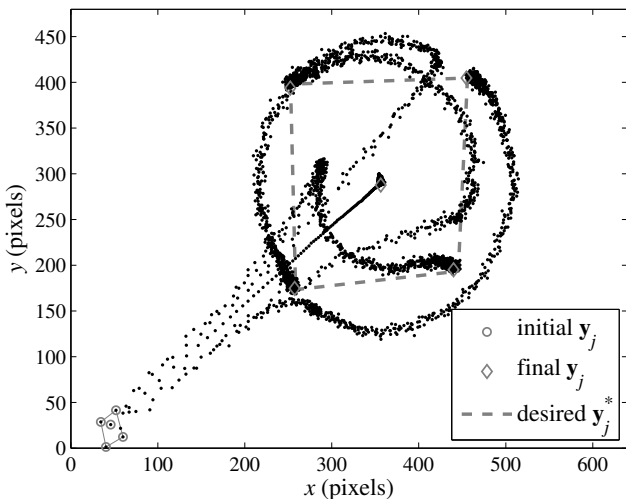
the plane Π with this upper face, we guarantee that the inertial position ${}^I \mathbf{p}(t)$ remains above the features, while converging to ${}^I \mathbf{p}^* = -R^{*T} \mathbf{p}^*$. This choice of feature geometry simplifies the process of recovering the rotation matrix R_e and the depth ratio α from images coordinates, since the 3-D reconstruction algorithm for planar scenes can be directly applied to the pairs (Y_1, X_1) and (Y_2, X_2) . In addition, as shown in Fig. 1, the points in X_1 can be interpreted as the vertices of a rectangle whose centroid lies at the intersection between the vectors $\mathbf{x}_3 - \mathbf{x}_1$ and $\mathbf{x}_4 - \mathbf{x}_2$. It follows that the image of the centroid also lies at the intersection between the vectors $\mathbf{y}_3 - \mathbf{y}_1$ and $\mathbf{y}_4 - \mathbf{y}_2$, and therefore \mathbf{y} can be readily obtained even though it is not the image of a feature point.

The simulation results that follow were obtained with the polyhedron parameters given by $a_1 = b_1 = 0.12$, $a_2 = b_2 = 0.14$, and $c = 0.04$, the control gains $k_1 = 0.5$, $k_2 = 1$, $k_3 = k_4 = 0.1$, and $k_z = 1$, and the eigenvalues $\lambda_1 = 0.8$, $\lambda_2 = 0.78$, and $\lambda_3 = 0.75$. The target

position and orientation were set to $\mathbf{p}^* = [0.05 \ 0.06 \ 1]^T$ and $R^* = \text{rot}(-0.4, [0.77 \ 0.63 \ -0.1]^T)$, respectively, yielding ${}^I\mathbf{p}^* = [-0.29 \ 0.23 \ -0.93]^T$. The corresponding set \mathcal{C} , which results from choosing $\mathbf{n}_\pi = [0 \ 0 \ -1]^T$, is shown in Fig. 7(a). The initial conditions were chosen



(a) 3-D trajectory



(b) 2-D trajectory in the image plane

Fig. 7. System trajectories.

so as to illustrate the performance of the proposed solution. With ${}^I\mathbf{p}(t_0) = [-4.5 \ 4.5 \ -3.8]^T$ m and $R(t_0) = \text{rot}(2.71, [0.22 \ -0.39 \ 0.89]^T)$, there is a large error in position and orientation, $\mathbf{p}_e(t_0) = [-2.59 \ -1.86 \ 5.73]^T$ m and $\theta_e(t_0) = 159$ deg, and the initial image is close to the borders of the FOV (see Fig. 7(b)). For the initial estimate of the desired depth, whose actual value was $z^* = 1$ m, we used $\hat{z}^*(t_0) = 1.5$ m.

The camera calibration matrix used in the simulations

is given by

$$A = \begin{bmatrix} \frac{f}{s_x} & -\frac{f \cot \theta}{s_x} & o_x \\ 0 & \frac{f}{s_y \sin \theta} & o_z \\ 0 & 0 & 1 \end{bmatrix}, \quad (25)$$

with the focal length $f = 8$ mm, the image center $(o_x, o_y) = (320, 240)$ pixels, the effective pixel size in x and y $(s_x, s_y) = (0.011, 0.01)$ mm, and the angle between axes $\theta = 90^\circ$. An error of 25% was added to f/s_x and f/s_y . Finally, the image update rate was set to 10 frames per second and the image measurements were corrupted with additive Gaussian noise with a standard deviation of 3 pixels.

Figure 7 illustrates the convergence behavior that can be achieved with the proposed two-stage controller. The first and second stages of the trajectory can be easily identified. While the first controller is being applied, the body rotates around itself to point to the target and moves approximately along a straight line until \mathbf{p}_e is close to zero (see Fig. 7(a)). This is projected into a translation and zooming in of the image coordinates \mathbf{y}_j in the image plane (see Fig. 7(b)). Regarding the second controller, which takes the body to its desired configuration, the resulting 3-D trajectory involves both rotational and translational motions, which can be approximately identified as a rotation of the feature points in the image plane. Figure 8 shows the position error \mathbf{p}_e and the angle for the rotation error θ_e as they converge to zero. The linear and angular velocity inputs are shown in Fig. 9 and 10, respectively.

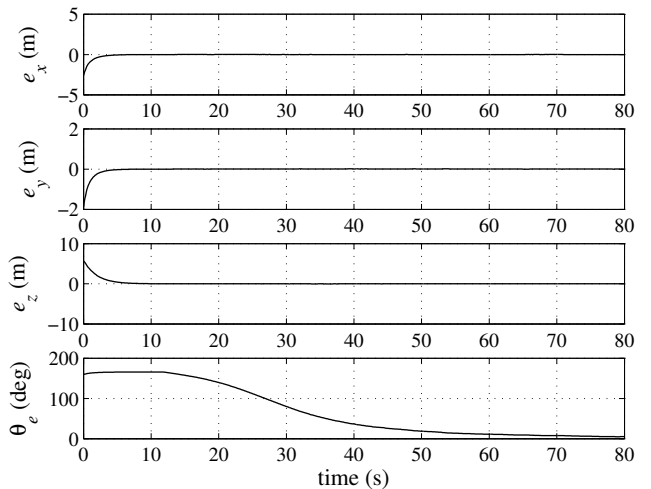


Fig. 8. Time evolution of the position error $\mathbf{p}_e = [e_x \ e_y \ e_z]^T$ and orientation error θ_e .

5 Conclusions

The paper presented a vision-based solution to the problem of stabilization on SE(3). Based on the image coordinates of a set of feature points and reconstructed

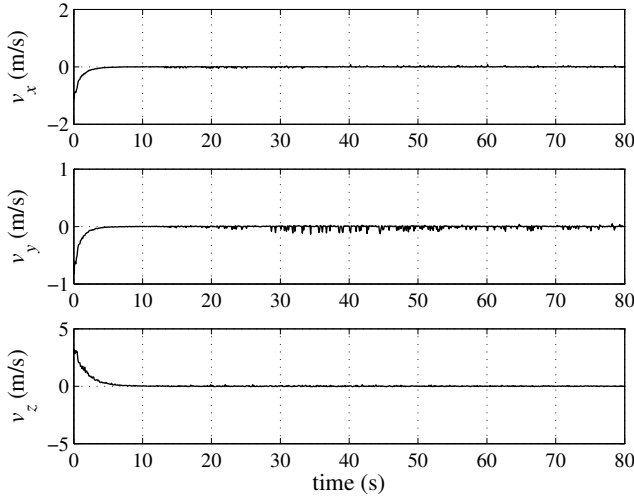


Fig. 9. Time evolution of the linear velocity $\mathbf{v} = [v_x \ v_y \ v_z]^T$.

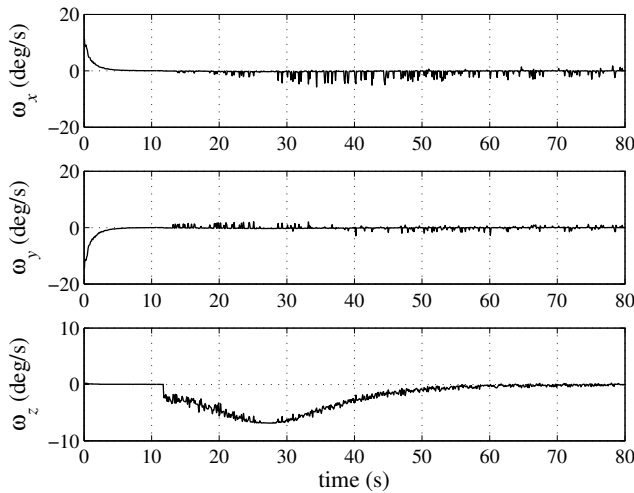


Fig. 10. Time evolution of the angular velocity $\boldsymbol{\omega} = [\omega_x \ \omega_y \ \omega_z]^T$.

rotation and depth information, a two-stage controller was defined to ensure that the features remain visible while the system converges to an almost global attractor. Necessary conditions for feature visibility were enforced, which include keeping the camera above the features and maintaining a feature point inside the FOV. Simulation results were presented, which support the adequacy of the proposed method.

Acknowledgments

This work was partially funded by Fundação para a Ciência e a Tecnologia (ISR/IST plurianual funding), through the PIDDAC Program funds and the projects HELICIM (PTDC/EEA-ACR/72853/2006) and SCARVE (PTDC/EEA-CRO/102857/2008), and by the NSF Grant CNS-0720842.

References

- Angeli, D., Jun. 2004. An almost global notion of input-to-state stability. *IEEE Transactions on Automatic Control* 49 (6), 866–874.
- Bhata, S. P., Bernstein, D. S., Jan. 2000. A topological obstruction to continuous global stabilization of rotational motion and the unwinding phenomenon. *Systems and Control Letters* 39 (1), 63–70.
- Bullo, F., Murray, R. M., 1999. Tracking for fully actuated mechanical systems: A geometric framework. *Automatica* 35 (1), 17–34.
- Chaturvedi, N., Bloch, A., McClamroch, N., Jun. 2006. Global stabilization of a fully actuated mechanical system on a riemannian manifold: controller structure. In: *Proceedings of the American Control Conference*. pp. 3612–3617.
- Chaturvedi, N., McClamroch, N., Bernstein, D., Jun. 2009. Asymptotic smooth stabilization of the inverted 3-D pendulum. *IEEE Transactions on Automatic Control* 54 (6), 1204–1215.
- Cheah, C. C., Liu, C., Slotine, J. J. E., Jun. 2010. Adaptive jacobian vision based control for robots with uncertain depth information. *Automatica*, in press.
- Chen, J., Dawson, D. M., Dixon, W. E., Chitrakaran, V. K., Jul. 2007. Navigation function-based visual servo control. *Automatica* 43 (7), 1165–1177.
- Chesi, G., Hashimoto, K., Prattichizzo, D., Vicino, A., Oct. 2004. Keeping features in the field of view in eye-in-hand visual servoing: A switching approach. *IEEE Transactions on Robotics* 20 (5), 908–913.
- Chesi, G., Vicino, A., Aug. 2004. Visual servoing for large camera displacements. *IEEE Transactions on Robotics* 20 (4), 724–735.
- Cowan, N. J., Weingarten, J. D., Koditschek, D. E., Aug. 2002. Visual servoing via navigation functions. *IEEE Transactions on Robotics and Automation* 18 (4), 521–533.
- Cunha, R., Silvestre, C., Hespanha, J., Aguiar, A. P., 2007. Vision-based control for rigid body stabilization. In: *Proceedings of the 2007 IEEE Conference on Decision and Control*. pp. 2345–2350.
- Cunha, R., Silvestre, C., Hespanha, J. P., Dec. 2008. Output-feedback control for stabilization on SE(3). *Systems & Control Letters* 57 (12), 1013–1022.
- Deng, L., Janabi-Sharifi, F., Wilson, W. J., Aug. 2005. Hybrid motion control and planning strategies for visual servoing. *IEEE Transactions on Industrial Electronics* 52 (4), 1024–1040.
- Espiau, B., Chaumette, F., Rives, P., Jun. 1992. A new approach to visual servoing in robotics. *IEEE Transactions on Robotics and Automation* 8 (3), 313–326.
- Faugeras, O., Lustman, F., 1988. Motion and structure from motion in a piecewise planar environment. *International Journal of Pattern Recognition and Artificial Intelligence* 2 (3), 485–508.
- Gans, N. R., Hu, G., Dixon, W. E., Sep. 2008. Simultaneous stability of image and pose error in visual servo control. In: *Proceedings of the IEEE Multi-conference*

- on Systems and Control. pp. 438–443.
- Gans, N. R., Hutchinson, S. A., Jun. 2007. Stable visual servoing through hybrid switched-system control. *IEEE Transactions on Robotics* 23 (3), 530–540.
- García-Aracil, N., Malis, E., Aracil-Santonja, R., Pérez-Vidal, C., Dec. 2005. Continuous visual servoing despite the changes of visibility in image features. *IEEE Transactions on Robotics* 21 (6), 1214–1220.
- Hamel, T., Mahony, R., Jul. 2007. Image based visual servo control for a class of aerial robotic systems. *Automatica* 43 (11), 1975–1983.
- Koditschek, D. E., 1989. The application of total energy as a lyapunov function for mechanical control systems. In: Marsden, J. E., Krishnaprasad, P. S., Simo, J. C. (Eds.), *Dynamics and Control of Multibody Systems*. Vol. 97 of *Contemporary Mathematics*. American Mathematical Society, pp. 131–158.
- Lopes, G., Koditschek, D., Jul. 2007. Visual servoing for nonholonomically constrained three degree of freedom kinematic systems. *The International Journal of Robotics Research* 26 (7), 715–736.
- Ma, Y., Soatto, S., Kosecka, J., Sastry, S., 2004. *An Invitation to 3-D Vision From Images to Geometric Models*. Vol. 26 of *Interdisciplinary Applied Mathematics*. Springer.
- Malis, E., Chaumette, F., Apr. 2002. Theoretical improvements in the stability analysis of a new class of model-free visual servoing methods. *IEEE Transactions on Robotics and Automation* 18 (2), 176–186.
- Malisoff, M., Krichman, M., Sontag, E., Apr. 2006. Global stabilization for systems evolving on manifolds. *Journal of Dynamical and Control Systems* 12 (2), 161–184.